Drag Reduction via Transversal Wave Motions of Structured Surfaces

Marian Albers

Institute of Aerodynamics
RWTH Aachen University
Wüllnerstraße 5a, 52062 Aachen
m.albers@aia.rwth-aachen.de

Pascal S. Meysonnat

Institute of Aerodynamics
RWTH Aachen University
Wüllnerstraße 5a, 52062 Aachen
p.meysonnat@aia.rwth-aachen.de

Wolfgang Schröder

Institute of Aerodynamics
RWTH Aachen University
Wüllnerstraße 5a, 52062 Aachen
office@aia.rwth-aachen.de

ABSTRACT

A combination of passive and active control methods is used to lower the friction drag in turbulent boundary layer flows. Both techniques, i.e. ribbed surfaces and spanwise traveling surface waves, have proven to reduce the skin friction significantly. Thus, a hybrid approach could lead to a higher drag reduction potential. In a high resolution large-eddy simulation (LES), the combined setup, i.e., the actuated ribbed surface, is compared against a reference smooth flat plate and the two seperate control methods. The results show a further increase of the drag reduction rate for the actuated riblets compared to the non-actuated riblets, and a similar drag level as in the actuated smooth setup. The streamwise turbulent intensities and the wall-normal vorticity are lowered in the crest and the trough region for both actuated cases.

Introduction

The drag and hence the energy-consumption of slender bodies moving in a fluid, e.g., an aircraft, is mainly determined by friction drag. For aircraft at cruise speed, the flow over the wing and body is largely in a turbulent state, thus, the major component of the fluid dynamical drag, i.e. about 50%, can be attributed to the viscous shear stress distribution. Consequently, there is considerable scientific interest in influencing the flow to gain net energy savings for more efficient transportation. Generally, the techniques to decrease the drag are divided into whether or not external energy is introduced into the system, i.e., passive and active methods are used to influence the drag.

Passive methods such as tiny grooves aligned in the streamwise flow direction, so-called riblets, were extensively investigated by Bechert *et al.* (1985). Ideally, the very sharp riblet tips shift the transverse no-slip condition away from the wall, thus weakening the turbulence regeneration cycle (Jiménez & Pinelli (1999)). About 10% drag reduction was found for a riblet width of $s^+ = 15 - 20$ in inner units (Bechert *et al.* (1997)). Furthermore, riblet structured surfaces can delay the transition to fully turbulent flow, since streaks in the streamwise direction are damped (Klumpp *et al.* (2010a)). However, for optimal energy savings the riblets have to be optimized for fixed operation points. That is, deviating from that optimal operating point results in a change of drag and eventually leads to drag increase.

In contrast, active techniques for the control of turbulent wall-bounded flows offer the possibilities to overcome the shortcomings of the passive techniques. That is, a change in operating point and therefore a change in drag, can be accounted for by changing the parameter of the actuation system. Numerous actuation methods have been developed and tested over the years such as influencing the near-wall flow structures by body forces, blowing and suction, or moving walls to achieve a beneficial drag effect. A general overview of various actuation methods is given in Quadrio (2011). For instance, Choi *et al.* (1998) conducted experiments in a wind tunnel using spanwise wall oscillation and achieved drag reduction rates of up to 45 percent. Quadrio *et al.* (2007) extended the idea by converting the temporal oscillation to a spatial one through streamwise traveling waves of spanwise wall velocity in a direct numerical simulation (DNS) of turbulent channel flow. Utilizing the convective nature of the flow improved the unsteady nature of the temporal oscillation technique and achieved maximum drag reduction rates of up to 48 percent. Often, the methods have shown excellent drag reduction rates and even net energy savings in experiments and numerical simulations. It remains a challenge, though, to implement these designs into any environment that resembles a wing profile or even a bare metal sheet, as it is often unclear how body forces can be applied to external air flows. Additionally, most often the investigations deal with channel flows, which represent a certain ideal configuration, since, unlike in turbulent boundary layers, no streamwise development of the quantities is present.

Therefore, spanwise traveling transversal surface waves have become a promising new approach to influence friction drag in wall-bounded turbulent flows. Early numerical works by Du & Karniadakis (2000) and Du *et al.* (2002) using spanwise traveling waves showed the efficiency and robustness of this approach. Zhao *et al.* (2004) substituted the previously used body force by an equivalent in-plane wall acceleration, reducing the turbulent drag by about 30 percent for channel flows at a Reynolds number $Re_\tau = 180$. The authors were optimistic that such flexible walls will be technically available in the near-future. Therefore, more recently Itoh *et al.* (2006) and Tamano & Itoh (2012) showed drag reduction of up to 13 percent in experimental setups by using spanwise traveling waves of wall-normal up and down motion. Note that these experiments were performed for an external flow, i.e., a turbulent boundary layer, in contrast to the previously mentioned channel flow investigations. These results were confirmed in principal in a high resolution LES of turbulent boundary layers by Klumpp *et al.* (2010b). The investigation of two distinct wave setups with different wave parame-

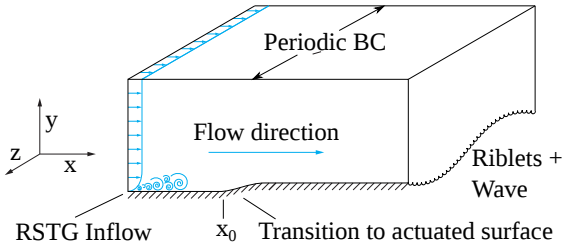

Figure 1: Schematic of the numerical setup of the actuated riblet surface.

ters, i.e., wavelength, period, and amplitude, yielded a differentiated drag behavior. Whereas the long wavelength ($\lambda^+ = 870$) reduced the drag significantly, the short wavelength ($\lambda^+ = 174$) showed a drag increase. By comparing both setups, which were excited by the same mechanism, Klumpp *et al.* (2010b) were able to show that the reduction of wall-normal vorticity is a key indicator for drag reduction. More recently, the effect of changing the amplitude in the range $A^+ = 30-70$ in inner units at increasing momentum thickness based Reynolds number ($1000 \leq Re_\theta \leq 7000$) on the drag reduction of a transversal traveling surface wave with a wavelength of $\lambda^+ = 500$ in inner coordinates was investigated by Koh *et al.* (2015). It was shown that increasing the amplitude can compensate the weakening of the drag reduction, observed at increasing Reynolds number. Furthermore, the reduction in wall-normal vorticity was also observed, confirming the hypothesis of Klumpp *et al.* (2010b). Moreover, the comparison between large-eddy simulation (LES) and experimental data shows excellent agreement (Meysonnat *et al.* (2016)).

An open question in the context of flow control for drag reduction is whether or not passive and active techniques can be positively combined, i.e., a superposition of the drag reducing effects exists. Admittedly, the non-linearity of the flow problem makes it highly unlikely that the savings of each technique can be simply added up. Therefore, in the present study a combination of riblets and transversal traveling surface waves is considered. The goal is to investigate how the two techniques will behave when combined and if they can coexists without canceling each other out.

Computational Setup

The investigations are performed numerically by an LES of a zero-pressure gradient turbulent flat plate boundary layer flow using riblet surfaces and transversal traveling surface waves. To investigate the effect of the riblets and the transversal traveling wave on the drag, four configurations are used in the current work, i.e., a smooth non-actuated reference case, a non-actuated riblet case, an actuated smooth transversal traveling surface wave, and an actuated riblet transversal traveling surface wave. A schematic of the computational domain is shown in Fig. 1. Like in the analysis of Koh *et al.* (2015) there is a smooth transition from the non-actuated to the actuated part of the flat plate allowing the synthetically prescribed flow to fully develop. This transition region, given by

$$y_{\text{wall}}(x) = \begin{cases} 0 & \text{if} \quad x \leq x_0 \\ \frac{A}{2}\left[1-\cos\left(\frac{\pi(x-x_0)}{3\theta_i}\right)\right] & \text{if} \quad x_0 \leq x \leq 3\theta_i \\ A & \text{if} \quad x \geq 3\theta_i, \end{cases}$$

is located at x_0 (cf. Fig. 1) which is approx. $\Delta x = 5\delta_0$ downstream of the inflow. The transversal traveling surface wave motion is given by

$$y^+|_{\text{wall}}(z^+,t^+) = A^+ \cos\left(\frac{2\pi}{\lambda^+}z^+ - \frac{2\pi}{T^+}t^+\right), \qquad (1)$$

where $\lambda^+ = \lambda u_\tau/\nu$ is the wavelength, $A^+ = Au_\tau/\nu$ is the amplitude, and $T^+ = Tu_\tau^2/\nu$ is the period. The plus superscript represents inner scaling defined by the friction velocity u_τ and the dynamic viscosity ν. The four flow setups, non-actuated smooth plate (SN), actuated smooth plate (SA), non-actuated riblets (RN), and actuated riblets (RA), have the same physical extent and identical wave parameters are used for the two actuated cases. The wavelength is $\lambda^+ = 1000$ and an amplitude of $A^+ = 30$ and a period of $T^+ = 40$ are used. The Reynolds number is $Re_\theta = 1.000$, where θ is the momentum thickness at x_0, and the Mach number of the flow is $Ma = 0.2$. The major difference between the setups is the wave surface, which is smooth for SN and SA and structured for RN and RA. The riblets used in the current investigation have an optimal spacing ($s^+ = 15$) to achieve a maximum drag reduction. The wavelength of the spanwise motion is kept large compared to the riblet size to avoid strong bending and deformation of the riblets. A summary of all relevant properties of the four setups is given in Tab. 1.

The simulations are first run for $t = \theta/u_\infty = 500$ convective time units until a quasi-steady state is observed in the integrated drag evolution. Samples for the reference case (SN) and the riblet only case (RN) are then gathered for another 800 convective time units, whereas in the actuated cases (FA and RA) the wave motion is started from zero by gradually increasing the amplitude to its target value. Once a new steady state is reached, the flow is sampled and averaged in a moving frame of reference.

Numerical Method

The numerical method is a high resolution large-eddy simulation (LES) solving the filtered compressible unsteady Navier-Stokes equation on curvilinear grids. For the convective fluxes the advection upstream splitting method (AUSM) is used, while a central scheme is employed for the viscous terms. The temporal integration is performed by an explicit 5-stage Runge-Kutta method, at second-order accuracy. An implicit LES model is used, following the approach of monotonically integrated LES (MILES) by Boris *et al.* (1992) such that the AUSM provides for the necessary dissipation for the smallest scales. Investigations by Meinke *et al.* (2002) have shown that no additional explicit turbulence model is required.

To avoid the simulation of the entire streamwisely developing boundary layer, that is the transition from laminar to turbulent flow, the reformulated synthetic turbulence generation (RSTG) method by Roidl *et al.* (2013, 2014) is used. The RSTG method prescribes a turbulent velocity field at the inflow of the domain by simulating virtual eddy cores encompassing the inflow plane. The fluctuation contribution of each eddy core is computed and superposed to the mean velocity components from a previous RANS computation, which was computed using the one-equation turbulence model by Fares & Schröder (2005). The approach allows adaptation lengths between the inlet plane and a fully statistical turbulent flow of less than three to four boundary layer thicknesses and thereby makes the overall computational method more efficient. In the spanwise direction, periodic boundary conditions are prescribed, at the outflow boundary condition the equations in their characteristic form are used. Additionally, a sponge layer is prescribed at the outflow to damp numerical reflections. At the wall the no-slip condition is applied.

Results

The effect of the active control, i.e., the spanwise traveling surface wave, on the smooth and riblet surface on the drag reduction is shown in Fig. 2. Especially the transient state is depicted, i.e., the time in which the actuation is ramped up from an initially non-actuated reference turbulent boundary layer. The drag reaches its new quasi-steady state value within $\Delta t = 150-200$ convective

Table 1: Parameters of the four different setups. The domain dimensions are non-dimensionalized with the momentum thickness θ at x_0, whereas the grid resolution and the control parameters are given in inner units.

Name	Control	$L_x/\theta_i \times L_y/\theta_i \times L_z/\theta_i$	$N_x \times N_y \times N_z$	Δx^+	$\Delta y^+\|_{\text{wall}}$	Δz^+	T^+	A^+	λ^+	$s^+_{riblets}$
SN (smooth non-actuated)	None	$262 \times 80 \times 21.8$	$1030 \times 134 \times 268$	12	0.85	3.75	-	-	-	-
SA (smooth actuated)	Active	$262 \times 80 \times 21.8$	$1030 \times 134 \times 286$	12	0.85	3.75	40	30	1000	-
RN (riblets non-actuated)	Passive	$262 \times 80 \times 21.8$	$1030 \times 134 \times 1073$	12	0.85	0.94	-	-	-	15
RA (riblets actuated)	Active + Passive	$262 \times 80 \times 21.8$	$1030 \times 134 \times 1073$	12	0.85	0.94	40	30	1000	15

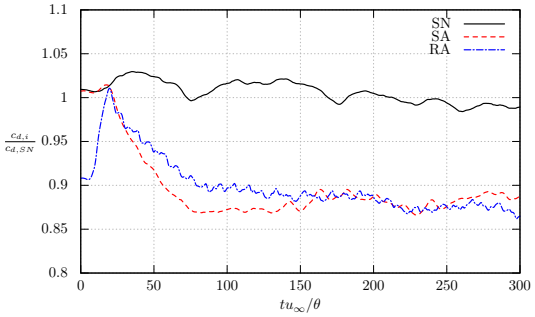

Figure 2: Comparison of the temporal transition of the integrated drag coefficient ratio $c_{d,i}/c_{d,SN}$ from non-actuated to actuated wall for the smooth (SA) and the riblet case (RA). The time evolution of the non-actuated smooth wall (SN) is shown for comparison.

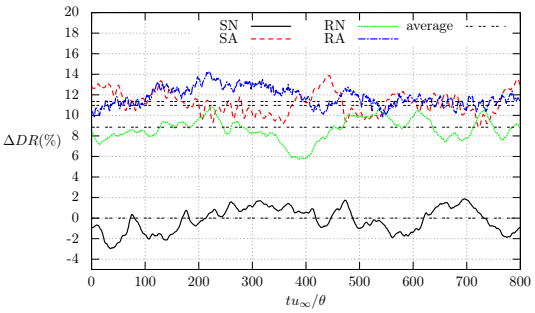

Figure 3: Comparison of the instantaneous drag reduction criterion *DR* for the four setups, where the non-actuated smooth surface (SN) is the reference. The corresponding temporal averages for each case are plotted with dashed lines.

times. Starting from the already lowered drag of the non-actuated riblet setup (RN), the distribution of the drag of the riblet wave (RA) shows a sudden temporary drag increase to a level comparable with the SN setup. Then, it recovers within 200 convective time to a new level below that from the SA setup.

A more detailed view on the actual drag reduction is given in Fig. 3, for the expression

$$\Delta DR = \frac{\int\limits_{A,\text{na}} \tau_{w,\text{na}} dA - \int\limits_{A,\text{ac}} \tau_{w,\text{ac}} dA}{\int\limits_{A,\text{na}} \tau_{w,\text{na}} dA} \qquad (2)$$

to compare the integrated drag of all controlled cases SA, RN, and RA with the drag from the uncontrolled case SN. Here, τ_w is the wall-shear stress and A is the wetted surface where the domain is fully actuated. Note that for the actuated setups the wetted surface increases, compared to the non-actuated flat plate, due to the sinusoidal form of the surface. Therefore, to accurately compare the drag between the different configurations, the surface increase has to be taken into account. Fig. **??** shows, that the average reduction for the integrated wall shear stress is 11% for the smooth actuated case, 8.8% for the riblet non-actuated case, and 11.4% for the riblet actuated case, compared to its reference case. That is, the drag of the actuated riblet surface is reduced by more than two percent, compared to the non-actuated setup (RN). However, the gain compared to the smooth actuated setup (SA) is small. Thus, a more detailed look at the distribution of the velocity gradients near the wall is necessary.

The wall-normal upward and downward motion of the wall by the transversal travling wave actuation induces a secondary flow field which is shown for the mean spanwise velocity component in Fig. 4. The maximal values are reached above the wave crest and minimal values in the trough region. Furthermore, the secondary flow field in the actuated riblet case is perturbed at the riblet tips upstream of the trough and the crest region.

The distribution of the phase- and time-averaged streamwise velocity component versus the wall-normal distance is shown in Fig. 5. All velocities are scaled by the friction velocity of the smooth non-actuated case (SN). The velocity of the SN case closely follows the theoretical distribution in the viscous sublayer and in the logarithmic region, proving the accuracy of the numerical method. For the actuated setups, the velocity is plotted above the crest and in the trough of the wave and for the riblet setups the velocity is plotted at the tip of the riblet and in the valley. In Fig. 5a the distribution over the whole boundary layer is shown for all configurations and a deviation from the curve of the SN setup can be seen for almost all setups. The velocity in the logarithmic region is increased for all three drag reduction setups, whereas a more differentiated analysis is necessary for the near-wall region, for which a zoom is given in 5b. The velocity above the crest of the SA setup is comparable to the SN case, in the trough region it is significantly lower, leading to a decreased velocity gradient at the wall. The distribution over the non-actuated riblet surface (RN) shows an increase of the velocity at the tip of the riblets and a reduction in the valley. In the trough region of the actuated riblet setup (RA) the velocity is lowered even further for the tip and the valley, whereas the velocity is only slightly increased at the riblet tips on the wave crest, lowering the combined drag of the trough and crest region. Overall, the actuation leads to a similar behavior for both, the smooth and the riblet surface, generally lowering the velocity gradients at the wall in the trough. In contrast, the velocity gradients at the crest only show little to no increase, thus confirming the positive effect of the wave motion on the turbulent flow field in the considered regions.

In Fig. 6 the root-mean-square (rms) values of the streamwise and spanwise velocity components are presented versus the wall-normal distance scaled by the friction velocity of the SN case. Comparing the distributions for both non-actuated cases SN and RN, it can be observed that the fluctuations for the streamwise and span-

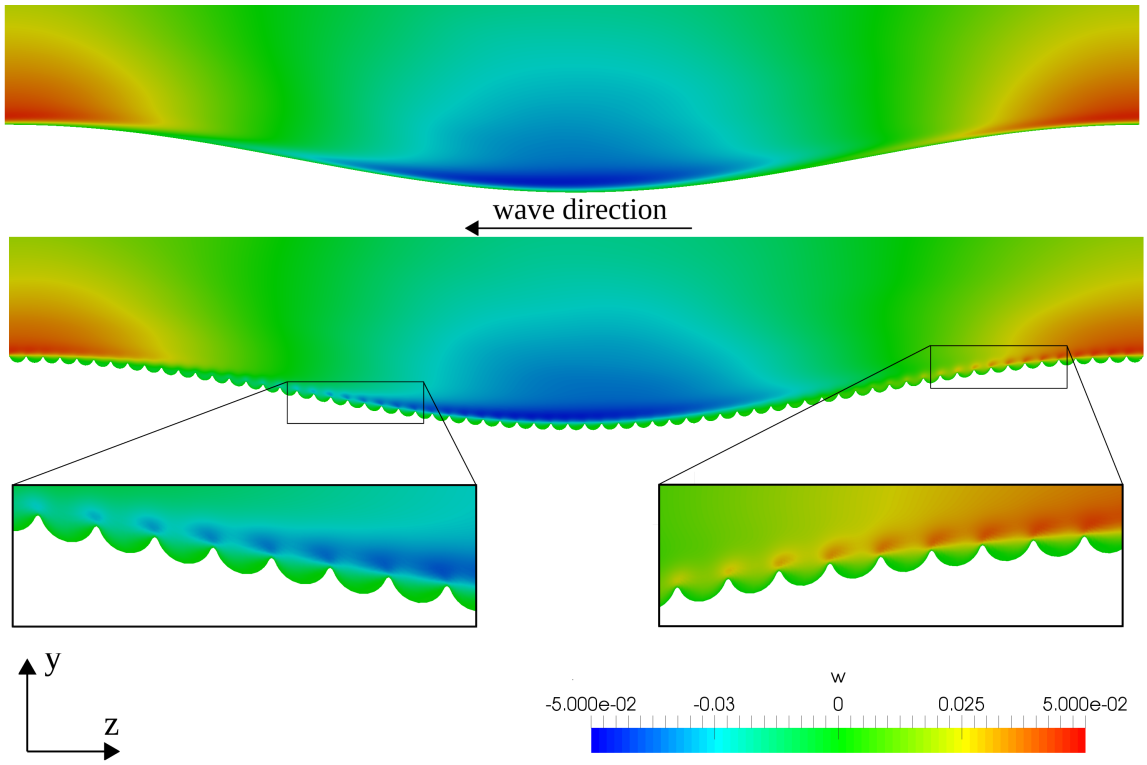

Figure 4: Secondary flow field of the spanwise velocity component in the $y-z$ plane for the actuated smooth setup (top) and the actuated riblet setup (bottom).

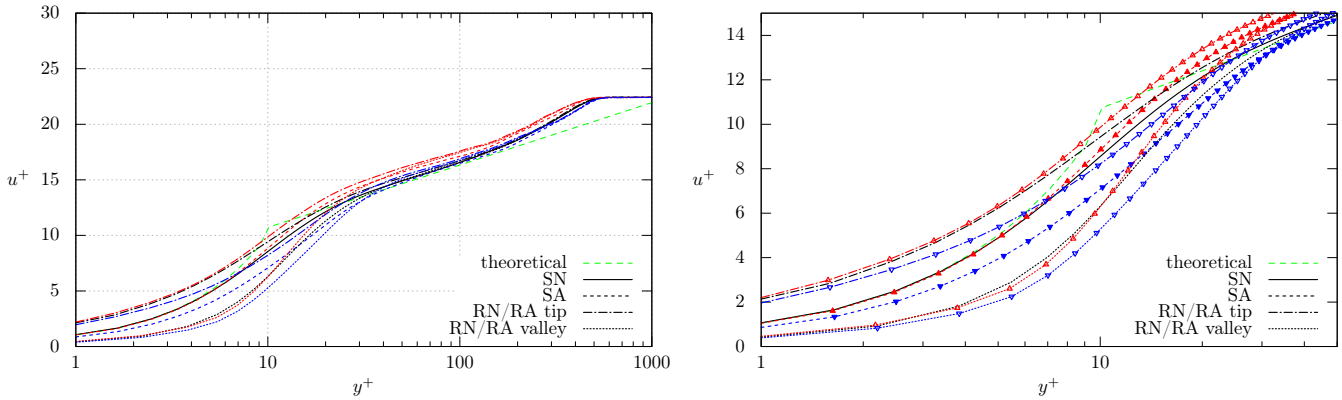

Figure 5: Phase averaged wall-normal distributions of the streamwise velocity component u scaled by the friction velocity of the smooth flat plate $u_{\tau,SN}$; (a) complete boundary layer, where ▲ and ▼ indicate values above the crest and in the trough region; (b) a detailed view of the near-wall region.

wise components are greatly reduced in the riblet valleys and increased at small distances above the tip. All distributions for the streamwise velocity of the actuated cases SA and RA in Fig. 6a are generally reduced in the near-wall region, compared to the non-actuated counterparts. The rms values of the spanwise velocity component in Fig. 6b show a decrease above the riblet tip of the actuated case RA close to the wall in the crest and the trough region, and an increase in the riblet valleys for the crest region. On average, the actuation yields lowered turbulent intensities for the smooth and the riblet surface.

The contours of the phase-averaged rms values of the streamwise vorticity component in Fig. 7 emphasize the perturbations at the riblet tips. These peaks of strong streamwise vorticity fluctuations are found to reach their maximum upstream of the trough and the crest region.

Finally, the wall-normal vorticity is considered which, according to Klumpp *et al.* (2010b) is a key indicator for drag reduction in turbulent boundary layers subjected to transversal traveling surface waves. The rms values of the wall-normal vorticity fluctuations versus the wall distance are shown in Fig. 8. For the non-actuated riblets RN, the values are increased above the tip and slightly decreased in the valley, although the influence is limited to small distances away from the wall. The active wave motion has a more

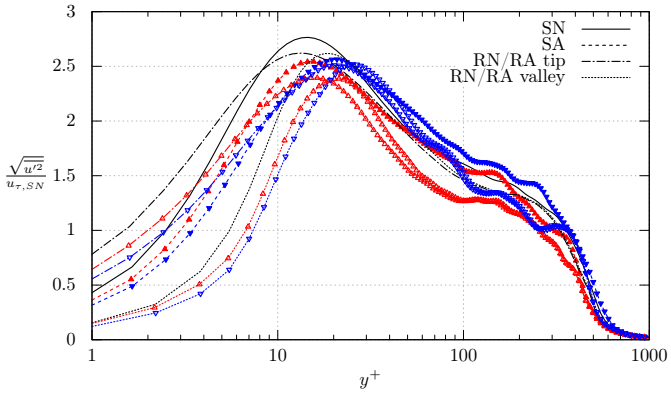

(a)

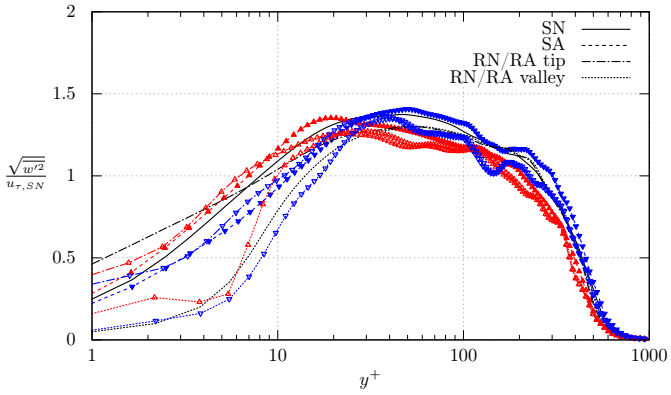

(b)

Figure 6: Phase-averaged wall-normal distributions of the velocity root-mean-square values scaled by the wall shear-stress of the smooth flat plate; (a) streamwise velocity component, where ▲ and ▼ indicate values above the crest and in the trough region; (b) rms values of the streamwise velocity component.

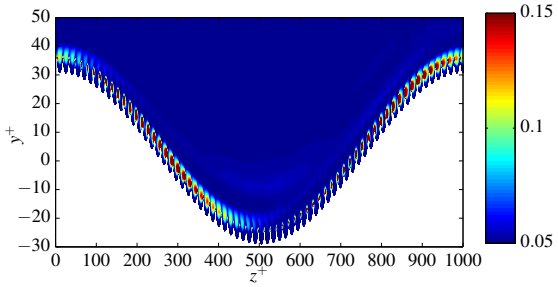

Figure 7: Contours of the phase-averaged root-mean-square of the streamwise vorticity component in the $y-z$ plane.

profound effect on the distributions. Generally, the vorticity fluctuations of the actuated setups are reduced at nearly all positions. The increase at the riblet tips can be only found for the region very close to the wall ($y^+ < 5$). At larger wall-normal distance the trend of the actuated smooth setup is followed.

Conclusion

Turbulent boundary layer flow controlled by passive and active methods and a combination of both was investigated using high-resolution LES. The flow was analyzed for a Mach number

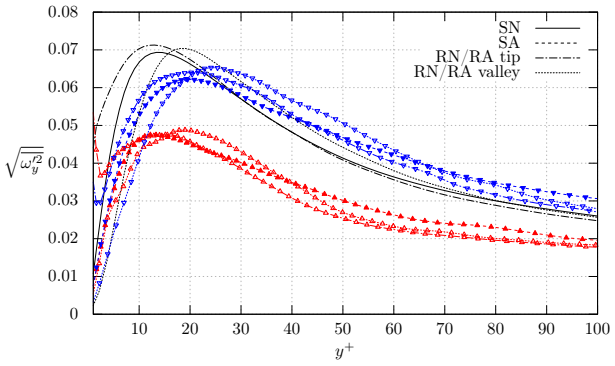

Figure 8: Phase-averaged wall-normal distributions of the wall-normal vorticity root-mean-square values, where ▲ and ▼ indicate values above the crest and in the trough region.

of $Ma = 0.2$ and a Reynolds number of $Re_\theta = 1{,}000$ based on the momentum thickness. A spanwise transversal traveling wave was applied to a smooth and a riblet structured surface. The phase- and time-averaged results were evaluated together with the corresponding non-actuated setups. The results show that the actuated riblet setup yields an increased drag reduction rate, compared to the non-actuated riblets, although only a slight gain can be achieved over the actuated smooth setup. One reason for this reduced gain is the secondary flow field in the spanwise direction, which interacts with the structured surface and causes new perturbations. This is illustrated in the streamwise vorticity fluctuation distribution which lowers the positive effect of riblets especially on the flanks of the wave. An analysis of the velocity distribution in the near-wall region of the crest and the trough reveals the positive effect of the wave motion flow field around the riblet surface, lowering the velocity in the trough region for the tip and in the valley, while being only slightly increased in the crest region. This trend is further confirmed by the decreased turbulent streamwise intensities close to the wall. Thus, the combination of an active and a passive method has shown to have a positive combined effect on velocity gradients and turbulent intensities. It is, however, unclear if a higher drag reduction rate can be gained from combinations of other control parameters, i.e., different amplitude and speed of the wave or resized riblets. Further investigations are necessary to achieve a better understanding of the physics in such a hybrid control method.

ACKNOWLEDGMENT

The authors would like to thank the Deutsche Forschungsgemeinschaft (DFG) for the funding of the research group FOR1779. Furthermore, the computing resources made available by the High-Performance Computing Center in Stuttgart (HLRS) and of the Jülich Supercomputing Center (JSC) along with their continued support are gratefully acknowledged.

REFERENCES

Bechert, D. W., Bruse, M., Hage, W., Hoeven, J. G. T. Van Der & Hoppe, G. 1997 Experiments on drag-reducing surfaces and their optimization with an adjustable geometry. *Journal of Fluid Mechanics* **338**, 59–87.

Bechert, D. W., Hoppe, G. & Reif, W.-E. 1985 On the drag reduction of the shark skin. *AIAA Paper* (85-0546).

Boris, J. P., Grinstein, F. F., Oran, E. S. & Kolbe, R. L. 1992 New insights into large eddy simulation. *Fluid Dynamics Research* **10** (4-6), 199.

Choi, K.-W., Debisschop, J.-R. & Clayton, B. R. 1998 Turbulent

boundary-layer control by means of spanwise-wall oscillation. *AIAA Journal* **36** (7), 1157–1163.

Du, Y. & Karniadakis, G. E. 2000 Suppressing wall turbulence by means of a transverse traveling wave. *Science* **288** (5469), 1230–1234.

Du, Y., Symeonidis, V. & Karniadakis, G. E. 2002 Drag reduction in wall-bounded turbulence via a transverse travelling wave. *Journal of Fluid Mechanics* **457**.

Fares, E. & Schröder, W. 2005 A general one-equation turbulence model for free shear and wall-bounded flows. *Flow, Turbulence and Combustion* **73** (3-4), 187–215.

Itoh, M., Tamano, S., Yokota, K. & Taniguchi, S. 2006 Drag reduction in a turbulent boundary layer on a flexible sheet undergoing a spanwise traveling wave motion. *Journal of Turbulence* **7**, N27.

Jiménez, J. & Pinelli, A. 1999 The autonomous cycle of near-wall turbulence. *Journal of Fluid Mechanics* **389**, 335–359.

Klumpp, S., Meinke, M. & Schröder, W. 2010a Numerical simulation of riblet controlled spatial transition in a zero-pressure-gradient boundary layer. *Flow, Turbulence and Combustion* **85** (1), 57–71.

Klumpp, S., Meinke, M. & Schröder, W. 2010b Drag reduction by spanwise transversal surface waves. *Journal of Turbulence* **11**, N22.

Koh, S.R., Meysonnat, P., Statnikov, V., Meinke, M. & Schröder, W. 2015 Dependence of turbulent wall-shear stress on the amplitude of spanwise transversal surface waves. *Computers & Fluids* **119**, 261–275.

Meinke, M., Schröder, W., Krause, E. & Rister, Th. 2002 A comparison of second-and sixth-order methods for large-eddy simulations. *Computers & Fluids* **31** (4), 695–718.

Meysonnat, P. S., Roggenkamp, D., Li, W., Roidl, B. & Schröder, W. 2016 Experimental and numerical investigation of transversal traveling surface waves for drag reduction. *European Journal of Mechanics - B/Fluids* **55**, 313323.

Quadrio, M. 2011 Drag reduction in turbulent boundary layers by in-plane wall motion. *Philosophical Transactions of the Royal Society A: Mathematical, Physical and Engineering Sciences* **369** (1940), 1428–1442.

Quadrio, M., Viotti, C. & Luchini, P. 2007 Skin-friction drag reduction via steady streamwise oscillations of spanwise velocity. In *Springer Proceedings Physics*, pp. 659–661. Springer Nature.

Roidl, B., Meinke, M. & Schröder, W. 2013 A reformulated synthetic turbulence generation method for a zonal RANS–LES method and its application to zero-pressure gradient boundary layers. *International Journal of Heat and Fluid Flow* **44**, 28–40.

Roidl, B., Meinke, M. & Schröder, W. 2014 Boundary layers affected by different pressure gradients investigated computationally by a zonal RANS-LES method. *International Journal of Heat and Fluid Flow* **45**, 1–13.

Tamano, S. & Itoh, M. 2012 Drag reduction in turbulent boundary layers by spanwise traveling waves with wall deformation. *Journal of Turbulence* **13**, N9.

Zhao, H., Wu, J.-Z. & Luo, J.-S. 2004 Turbulent drag reduction by traveling wave of flexible wall. *Fluid Dynamics Research* **34** (3), 175–198.